Transportation Geotechnics 43 (2023) 101138

Contents lists available at ScienceDirect

Transportation Geotechnics

journal homepage: www.elsevier.com/locate/trgeo

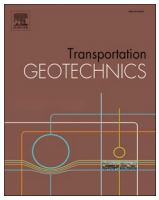

A simple method to determine soil–water retention curves of compacted active clays

Ana Sofia Dias [a,*], Paul N. Hughes [a], David G. Toll [a], Stephanie Glendinning [b]

[a] Department of Engineering, Durham University, Durham, UK
[b] School of Engineering, Newcastle University, Newcastle Upon Tyne, UK

ARTICLE INFO

Keywords:
Soil–water retention curve
Shrink-swell behaviour
Active clay
Compacted soil
Moisture cycles

ABSTRACT

Determining the Soil Water Retention Curve (SWRC) of an active clay constitutes a challenge due to the significant, and sometimes irreversible, volume changes that occur during wetting and drying cycles. A novel yet simple method of experimentally determining the evolution of the SWRCs with moisture cycles is presented based on the results of a rigorous experimental study. Its purpose is to support the modelling of water flux in earthworks exposed to weather cycles that cause deterioration. Firstly, three SWRC branches (the primary drying, a scanning drying, and a scanning wetting branch) are measured and used to fit the proposed generic SWRC semi-empirical model in terms of water ratio, that, in the adsorptive region, is independent of the compaction conditions (void ratio and water content at compaction). Soil Shrink-Swell Curves (SSSCs) in terms of water ratio versus void ratio, that are easy to measure, can be determined for different compaction conditions over several drying and wetting cycles. Finally, the SSSCs are combined with the generic SWRC model to determine the evolution of the SWRCs with moisture cycles for the compaction conditions of interest. This method is demonstrated for two London clays of high and very high plasticity. Samples were compacted in five different conditions, varying in gravimetric water content and dry density, and were cycled six times between 1 and 80 MPa of total suction. The generic SWRC model was fitted to the experimental data. The model was able to estimate the SWRC in terms of degree of saturation over the six drying-wetting cycles without propagation of error. The significance of the research is that SWRC can now be determined over a range of wetting and drying cycles quickly and simply and enable modelling of deterioration of clays fills due to the action of weather to be accurate.

Introduction

Earthworks are an important component of infrastructure, essential to our society and economy. Disruptions caused by the failure of earthworks lead to significant negative social and economic impacts within the UK and internationally. The economic costs can be high; annual expenditure on routine maintenance for earthworks on the UK railway network was £154 million in 2016/2017 and £111 million in 2017/2018 [1,2]. In order to reduce such losses, our understanding of the unsaturated soil behaviour of engineered fill used in earthworks must be improved, especially under changing climatic conditions [3–6]. A key soil property in the modelling of unsaturated soil behaviour is the soil–water retention curve (SWRC), which relates water content or degree of saturation to suction [7].

Embankments and cuttings are exposed to the atmosphere and are subjected to variations in water content due to cycles of rainfall and evaporation. SWRCs, commonly used in the modelling of soil slopes are represented in terms of degree of saturation or volumetric water content, which take into account the volume changes occurring during wetting and drying. Postill et al. [8–10] and Rouainia et al. [11] are some examples of studies on slope stability for which a volume dependent SWRC was essential.

A variety of methods have been used for SWRC measurement accompanied by volumetric deformations. In all methods, the suction is either applied (e.g., axis translation technique, vapour equilibrium technique, etc) or measured (e.g., tensiometer, filter paper technique, etc), while changes in water content are monitored using a balance. The volumetric deformations can be measured axially in an oedometer ring

* Corresponding author at: Department of Engineering, Durham University, Lower Mountjoy, South Road, Durham DH1 3LE, UK.
E-mail addresses: ana.s.dias@durham.ac.uk (A.S. Dias), paul.hughes2@durham.ac.uk (P.N. Hughes), d.g.toll@durham.ac.uk (D.G. Toll), stephanie.glendinning@ncl.ac.uk (S. Glendinning).

https://doi.org/10.1016/j.trgeo.2023.101138
Received 27 April 2023; Received in revised form 10 October 2023; Accepted 16 October 2023
Available online 18 October 2023

[12–14], or axially and radially accounting for the soil anisotropic behaviour [15,16]. Alternatively, methods have been developed that allow the prediction of the SWRC based on limited information on the soil-shrinkage curve [17,18].

Further challenges in the quantification of SWRCs of active clays come from the changes occurring over several cycles of wetting and drying. When soil is subjected to drying-wetting cycles, the SSSCs show accumulation of deformations, which depend on the compaction conditions and on the intensity of the drying-wetting cycles [19–21]. Therefore, a need for the development of a method that facilitates the quantification of the evolution of SWRCs over cycles of drying and wetting for different compaction conditions was identified.

The initial compaction conditions heavily influence the soil macro-porosity, which in turn controls the SWRC shape. However, when variations of water content occur within the micro-pores (within the aggregations of a compacted soil), different compaction conditions do not result in different SWRCs expressed in terms of water ratio or gravimetric water content, because volumetric deformations are decoupled from the retention behaviour [13,22–25]. This is the case when SWRCs are represented in terms of gravimetric water content (ratio between mass of water and mass of dry soil) or water ratio, e_w (ratio between volume of water and volume of solid particles).

In this paper, a generic SWRC relationship in terms of water ratio (SWRC-e_w) in the absorptive region is proposed, which can be calibrated on a limited amount of experimental data, requiring the measurement of three branches of the SWRC: primary drying, scanning wetting, and scanning drying. The generic SWRC-e_w can then be combined with soil shrink-swell curves (SSSCs; the relationship between void ratio and water ratio) to infer the SWRCs in terms of degree of saturation (SWRC-S_r) and their evolution with cycles of drying and wetting. The SSSCs are easy to measure, which makes the proposed method accessible and expeditious.

Moreover, in order to improve our understanding of the effect of different compaction conditions on the evolution of SSSCs, an extensive and unique dataset was developed in the present study. London Clay of different plasticity (high plasticity and very high plasticity) was tested. Samples were compacted at five different conditions varying the water content ($w = 0.20$ to 0.24) and dry density ($\gamma_d = 1.42$ to 1.52 Mg/m^3) relative to the Proctor optimum water content [26] to obtain a variety of initial states. The soil was subjected to six cycles of drying and wetting, between 1 and 80 MPa of suction. The total suction, water content and sample volume change were measured.

Experimental methods and materials

Materials

The present study was conducted on London Clay from two different locations in London (UK): Clapham (high plasticity) and Vauxhall (very high plasticity), for which properties are summarized in Table 1 [26]. X-ray diffraction analysis shows that both clay samples contain similar fractions of the same clay minerals (Illite, Smectite, and Kaolinite). However, the clay from Vauxhall presented higher clay content (54 %) than the clay from Clapham (41 %), which explains its higher plasticity.

Experimental methods

The clays were air-dried in the laboratory at a temperature of 20 ± 2 °C and a relative humidity of approximately 50 %, reaching a gravimetric water content of approximately 5 %. The fraction that passed through a 2 mm sieve was mixed with distilled water to obtain the desired water content (Table 2). The samples were statically compacted in a brass mould with a smooth finish to a diameter of 15 mm and a height of 5 mm, which dimensions were selected to fit the laboratory equipment for the measurement of suction, which limits the height of the samples to approximately 5 mm. The material was compacted in a single layer along the height of the sample. Due to the fine texture of the clay, the small sample is still representative of unsaturated hydraulic behaviour of the clay material in the range of tested suction values. The samples were extruded from the mould using a piston and placed in individual sealed capsules.

Table 1
Properties of the tested clays: plasticity classification, origin, specific gravity, particle size distribution, Atterberg limits, mineralogy from X-ray diffraction analysis, and Proctor compaction maximum density and optimum water content [26].

Plasticity classification		High plasticity	Very high plasticity
Origin (location)		Clapham	Vauxhall
Specific gravity		2.77	2.78
Particle size fractions	Clay (%)	41	54
	Silt (%)	49	42
	Sand (%)	10	4
Atterberg limits	Liquid limit (%)	60	77
	Plasticity Index (%)	36	53
Mineralogy of < 2 μm clay (X-ray diffraction)	Illite (%)	56	58
	Kaolinite (%)	17	16
	Chlorite (%)	6	6
	Smectite (%)	21	20
Proctor compaction	Optimum water content (%)	22	22
	Maximum dry density (Mg/m^{-3}(−|-))	1.58	1.59

The samples were compacted at five different conditions relative to the Standard Proctor optimum and maximum dry density, varying the water content (0.20–0.24) and the dry density (1.42–1.72 Mg m^{-3}) as detailed in Table 2. The optimum water content and the maximum dry density, reported in Table 1, were obtained from Standard Proctor compaction tests [26]. The sample compacted at Proctor optimum water content and maximum dry density are referred to as 'optimum'. The samples compacted at the same density as 'optimum' but on the wet- and dry-side in terms of water content are referred to as 'wet' and 'dry', respectively. Samples compacted at the Proctor optimum water content, but at a higher and lower density than 'optimum' are referred to as 'dense' and 'loose', respectively. In summary, a total of ten samples were compacted, i.e., five samples per clay type as reported in Table 2 ('loose', 'optimum', 'dense', 'wet', and 'dry' for high plasticity and very high plasticity London clay).

The quantification of the soil water retention curves (SWRCs) and of the shrinkage curves was performed by measuring the suction, water content and void ratio in the samples over six cycles of drying and wetting phases. In this way, six drying SWRCs and six wetting SWRCs were measured per sample. The total suction was measured using a chilled mirror dew point potentiometer WP4C [27] with an accuracy of ± 0.05 MPa from 0 to 5 MPa and 1 % from 5 to 300 MPa. The chilled mirror dew point potentiometer WP4C was calibrated and used as suggested by Cardoso et al. [28] for optimized performance. The gravimetric water content was determined from variations in the sample weight measured using a balance with a precision of 0.0001 g. The changes in void ratio were measured by recording variations in the height and diameter of the sample at two locations using a digital calliper (accuracy of 0.01 mm). The measurements were made regularly during drying and wetting phases over a range of 1 to about 80 MPa to determine the drying and the wetting branches of the SWRC respectively.

The drying-wetting cycles imposed on the samples to measure the SWRCs started d with a drying phase. The suction at the end of each drying and wetting phase is presented in Fig. 1 for each sample. The drying phase was imposed by exposing the samples to air for approximately 20–30 min before each measurement. The drying phase ended when the measured total suction reached 80 MPa. The wetting phase was conducted by adding distilled water gradually with a syringe on the

Table 2
Initial properties of the samples for each clay for each compaction condition: void ratio (e), gravimetric water content (w), water ratio (e_w), degree of saturation (S_r), and total suction (s).

Clay	State of compaction	Void ratio, e	Gravimetric water content, w	Water ratio, e_w	Degree of saturation, S_r	Total suction, s (MPa)
High plasticity (HP)	loose	0.95	0.22	0.60	0.63	1.75
	optimum	0.77	0.22	0.60	0.78	1.58
	dense	0.64	0.22	0.60	0.94	1.78
	wet	0.77	0.24	0.66	0.85	1.53
	dry	0.75	0.20	0.55	0.74	1.22
Very high plasticity (VHP)	loose	0.95	0.21	0.59	0.62	1.11
	optimum	0.76	0.21	0.59	0.77	1.50
	dense	0.62	0.21	0.59	0.94	1.51
	wet	0.77	0.24	0.65	0.85	1.21
	dry	0.79	0.20	0.55	0.69	2.28

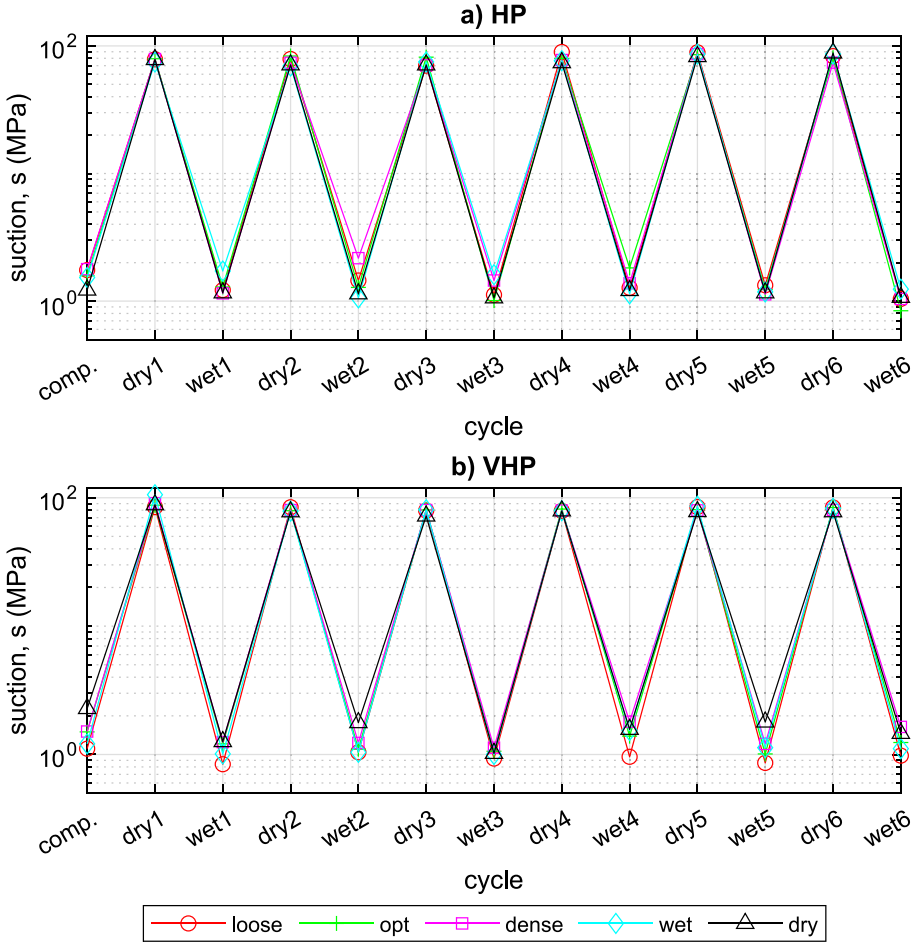

Fig. 1. Range of the imposed cycles of drying and wetting on the high plasticity (HP) and very high plasticity (VHP) London Clay samples during the measurement of SWRCs and SSSCs.

surface of the samples (0.01–0.02 g of water per step). The wetting phase ended when the total suction was approximately 1 MPa (Fig. 1). The measurements were performed after storing the samples in a sealed WP4C capsules for at least 30 min to allow the water to redistribute within the sample. A period of 30 min was observed to be enough for the suction measurement to stabilize after water content changes were imposed.

The storage of the samples during longer periods of time (e.g., overnight) may lead to loss of water because the WP4C capsules may not be perfectly sealed. During the drying phases, this loss of water is not significant enough to disturb the measurement of the SWRCs so the WP4C capsules containing the soil samples were simply placed in an air-tight container. In the wetting phase, the loss of water can result in an increase in suction (an inversion in the path direction) that is most significant when the suction is below 10 MPa. In this case, the WP4C capsules were stored in an air-tight container with wet tissue to keep a high humidity surrounding the samples.

Generic soil–water retention curves

Modelling of generic soil–water retention curves

The representation of the SWRC excluding the effect of volume changes can be made in terms of water ratio ($e_w = V_w/V_s$) or gravimetric water content. In the range of water content in which the water movement is governed by the intra-aggregate clay structure, the SWRC does

not depend on the density at compaction [13,22,24,29,30]. In this range, the water is found in the adsorptive regime, whereas at higher water contents, the water is found in the capillary regime.

Chen and Lu [31] presented an empirical relationship between the maximum adsorption water ratio, which represents the boundary between the capillary and adsorption regimes, and the clay size content of a wide variety of soils. The clay content of the HP and VHP clays are 41 % and 54 %, respectively, which equates to a maximum adsorption water ratio of 0.36 and 0.52 according to the relationship found by Chen and Lu [31]. Due to the evolution of the SWRCs with moisture cycling, the maximum water ratio is the initial one reported in Table 2. This way, the moisture cycle is expected to occur within the adsorptive regime in sample 'dry' of HP. However, for the remaining HP samples, 'loose', 'optimum', 'dense' and 'wet', the starting condition is predicted to be within the capillary regime. This possibility will be taken into account in the analysis of the results. The moisture cycle imposed on the VHP clay is expected to be always in the adsorptive regime.

Another study helped confirming that the water movement was dominated by the adsorptive regime. Monroy et al. [32] assessed the effect of wetting on the pore-size distribution through the analysis of Mercury Intrusion Porosimetry (MIP) tests. They compacted samples of London Clay at a gravimetric water content of 0.24 and void ratio of 0.95, which is comparable to the 'loose' samples of the present study. It was observed that wetting the compacted clay, from compaction (suction of 1000 kPa) to full hydration (suction of 0 kPa), leads to a decrease of the size of the inter-aggregate pore and an increase of the intra-aggregate pore size. The double-porosity was maintained until suctions were as low as 40 kPa.

Based on the Jurin-Laplace Law, the diameter of the pore correspondent to a suction of 1 MPa is 0.3 μm. It can be observed in the MIP test results of Monroy et al. [32] that the intra-aggregate pore-size at a suction of 1 MPa (0.1 μm) is lower than the above mentioned diameter, and the inter-aggregate pore-size of 11.68 μm is well above 0.3 μm. Therefore, the suction variations above 1 MPa tested in the present study are expected to be associated to water movement in the adsorptive regime.

Based on these arguments, a SWRC-e_w relationships are derived to describe the soil behaviour of compacted clay in the adsorptive regime. This is here referred to as the generic SWRC-e_w based on the conceptual model of Toll [33]. A semi-empirical model is then proposed, using the soil shrink-swell curves (SSSCs) to create SWRCs in terms of degree of saturation (SWRC-S_r), including the full volumetric effects of wetting and drying cycles. This semi-empirical model uses curve fitting in parts but is constrained by physical requirements, such as the end and start of a cycle having to match and the fact that the water ratio cannot exceed the void ratio.

The primary drying SWRC describes the soil going through its first drying phase. When the soil is re-wetted and re-dried, the state of the soil is described by scanning wetting and scanning drying SWRCs, respectively, that are less steep than the primary drying SWRC. The scanning wetting and scanning drying SWRCs are different due to hysteresis [34]. The scanning drying SWRC is less steep than the primary drying SWRC, therefore if upon drying the scanning drying SWRC intersects the primary drying SWRC, the primary drying SWRC then characterizes the state of the soil [33].

Fig. 2 presents an illustrative example of a simulated cycle starting from the compaction conditions: the first drying, first wetting, and second drying phases. The first drying phase is described by the primary drying SWRC ('drying 1′ in Fig. 2). When the sample is re-wetted ('wetting 1′ in Fig. 2), the scanning wetting SWRC defines the soil behaviour. The scanning drying SWRC characterizes the second drying phase of the soil from point C to D ('drying 2′ in Fig. 2), which is different from the scan wetting SWRC due to hysteresis. Upon re-drying, when the scanning drying SWRC intersects the primary drying SWRC (point D in Fig. 2), then further drying is characterized by the primary drying SWRC ('drying 2′ from point D to E in Fig. 2).

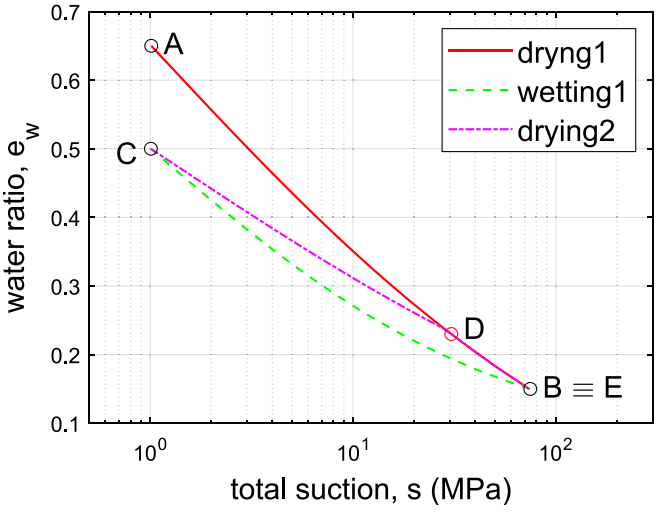

Fig. 2. Example of the estimation of two drying-wetting cycles using the generic soil–water retention curve model in terms of water ratio (SWRC-e_w) starting from the compaction conditions (point 1).

A sigmoidal function was adopted to allow the proper fitting to the slight curvature of the SWRC-e_w of three different curves: a primary drying ('drying 1′ in Fig. 2), a scanning wetting ('wetting 1′ in Fig. 2), and a scanning drying SWRC ('drying 2′ from point C to D in Fig. 2). The model forces the starting condition of each phase to be the reversal point, i.e., the point of the transition from drying to wetting or vice-versa (points B and C in Fig. 2).

The primary drying phase is described by Eq. (1), where e_w is the water ratio, s is the suction, a_1, b_1 and n_1 are fitting parameters (a_1 controls the position of the curve, and b_1 and n_1 control the slope and shape of the curve), and $\overline{e_{wi}}$ is the mean water ratio of all the samples at compaction to cancel the effects of the different water content at compaction of the samples and facilitate the fitting. The scanning wetting phases are described by Eq. (2), which depends on the estimated suction value of the reversal point (s_i), and requires the additional fitting parameters b_w and n_w. The scan drying phases, described by Eq. (3), depend on the reversal point (s_i) and on the reversal point of the wetting phase previous to that (s_{i-1}). For example, to describe the phase 'wetting 1′ in Fig. 2, the s_i value is that of point B. To describe the phase 'drying 2′ from point C to D, which is a scanning drying phase, the values s_i and s_{i-1} correspond respectively to points C and B, which are the final and initial suction values of the previous wetting phase ('wetting 1′). It is worth pointing out that the number of reversal points that is necessary to keep memory of does not increase with the number of cycles.

$$e_w = \overline{e_{wi}} - a_1 + \frac{b_1}{1 + s^{n_1}} \tag{1}$$

$$e_w = \overline{e_{wi}} - a_1 + \frac{b_1}{1 + s_i^{n_1}} - \frac{b_w}{1 + s_i^{n_w}} + \frac{b_w}{1 + s^{n_w}} \tag{2}$$

$$e_w = \overline{e_{wi}} - a_1 + \frac{b_1}{1 + s_{i-1}^{n_1}} - \frac{b_w}{1 + s_{i-1}^{n_w}} + \frac{b_w}{1 + s_i^{n_w}} - \frac{b_d}{1 + s_i^{n_d}} + \frac{b_d}{1 + s^{n_d}} \tag{3}$$

Fitting of the generic soil–water retention curve model

The SWRCs were measured over six drying-wetting cycles in each of the 10 tested samples, i.e., six drying SWRCs and six wetting SWRCs per sample. The SWRCs-e_w are represented in Fig. 3 grouped into primary drying ('drying 1′), scan wetting ('wettings 1 to 6′) and scan drying ('dryings 2 to 6′), and respective fitted generic SWRCs. The model was fitted in three different stages: (i) fitting of the parameters associated with the primary drying phases (phase 'drying 1′), (ii) fitting of the

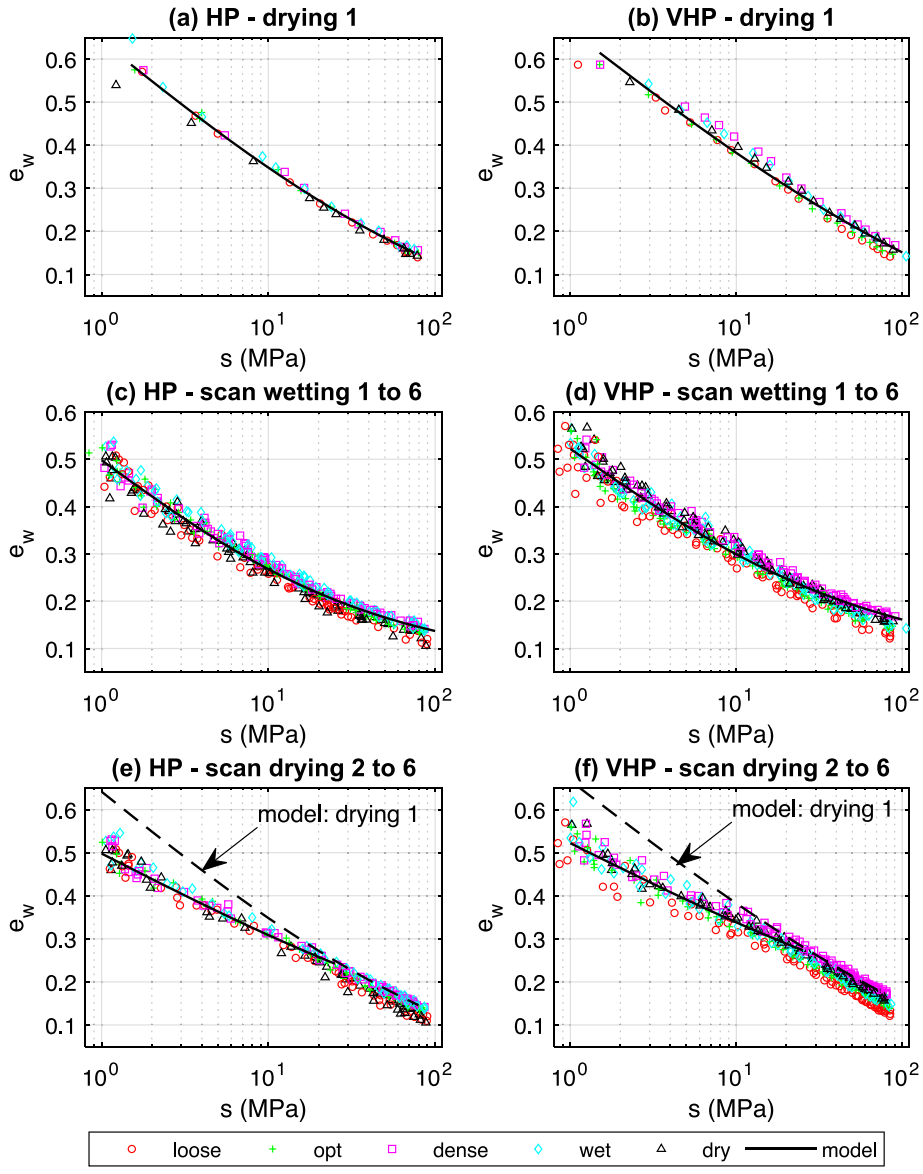

Fig. 3. Soil-water retention curves of high and very high plasticity clay (HP and VHP, respectively): primary drying phase (a, b), scanning wetting phases (c, d), and scanning drying phases (e, f).

parameters associated with all the scanning wetting phases (phases 'wetting 1 to 6'), and (iii) fitting of the parameters associated with all the scanning drying phases (phases 'drying 2 to 6'). The fitting was performed using a non-linear least-square fitting merging the data of all the samples of a given clay. Table 3 presents the fitting parameters for each clay and the coefficient of determination (R^2) of the fitting of each phase.

Table 3
Fitting parameters of the generic SWRC (Eq. (1) to (3).

Clay	High plasticity (HP)	Very high plasticity (VHP)
$\overline{e_{wi}}$	0.4650	0.4835
a_1	0.6000	0.7000
b_1	1.55529	1.7664
n_1	0.3453	0.2901
b_w	0.8766	0.9189
n_w	0.5071	0.4598
b_d	1.1389	1.1062
n_d	0.3000	0.3000
R^2 : drying 1 (primary)	0.988	0.982
R^2: scan wetting	0.977	0.969
R^2 : scan drying	0.967	0.927

The data relevant to obtain the fitting parameters associated with the primary drying phase is presented in Fig. 3a,b. The entire data set represented in Fig. 3c,d was used to obtain the fitting parameters of the scan wetting phase (Eq. (2). For simplicity, only the scan wetting curve assuming $s_i = 80MPa$ was represented in Fig. 3c,d. The values of suction lower than 30 MPa were used to fit the scan drying SWRC (Eq. (3) because the scanning drying SWRCs were observed to meet the primary drying at approximately that value, as observed in Fig. 3e,f. The scanning drying SWRC assumes $s_{i-1} = 80MPa$ and $s_i = 1MPa$ in Fig. 3e,f (only one curve is presented for simplicity).

Discussion on generic soil–water retention curves

The experimental SWRCs-e_w presented in Fig. 3 show that all samples of a given plasticity clay are very similar over the entire range. Fig. 4a-d presents the evolution of the initial and final water ratio of each drying phase ($e_{w,i}$ and $e_{w,f}$, respectively) to assess in more detail differences between samples and clay plasticity, and the evolution of the SWRCs-e_w with cycling. The initial and final water ratio of three drying

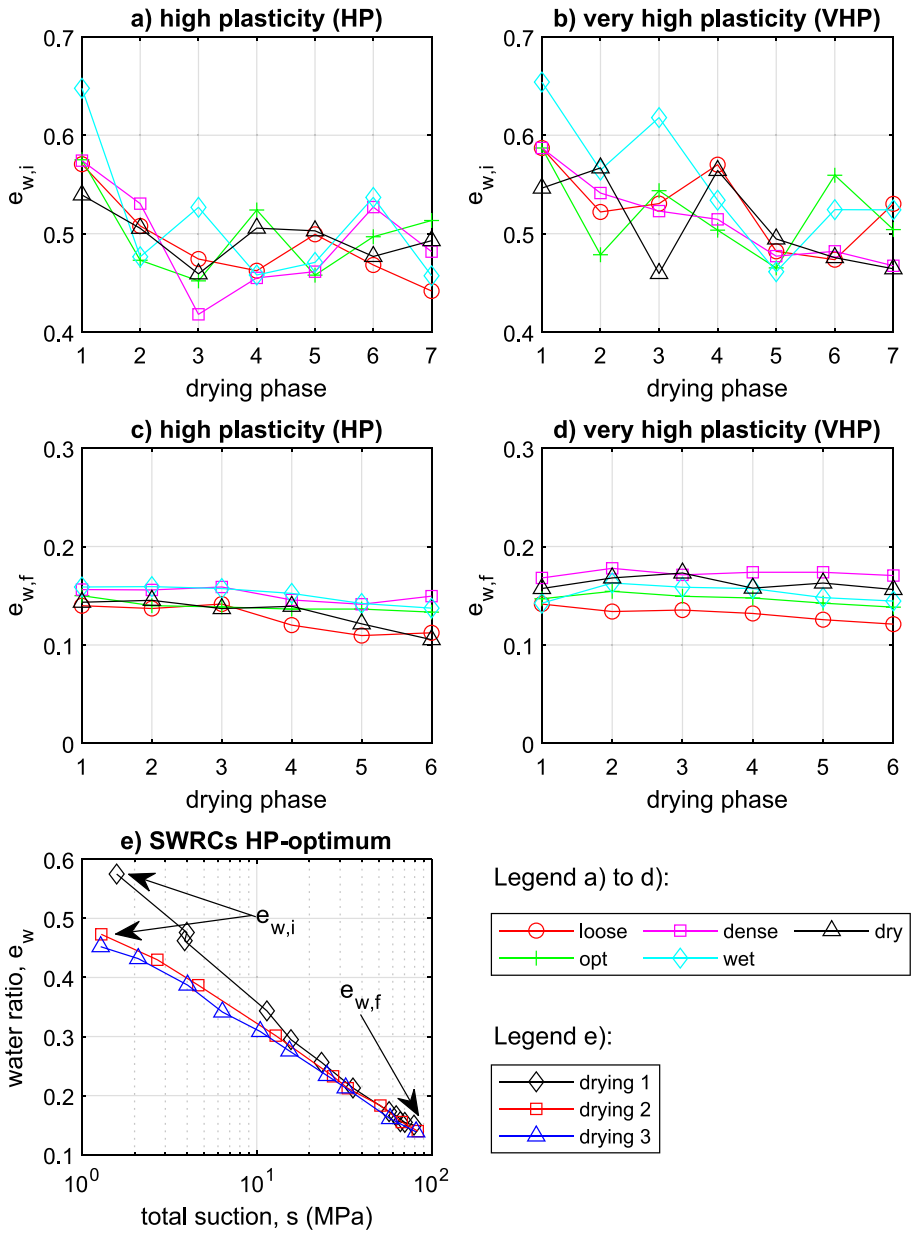

Fig. 4. Evolution of the (a, c) initial and (b, d) final water ratio, respectively $e_{w,i}$ and $e_{w,f}$, of each drying phase of samples of High Plasticity (HP) clay (left) and Very High Plasticity (VHP) clay (right) compacted at different conditions. Illustration of $e_{w,i}$ and $e_{w,f}$ for three drying phases of the sample "optimum" of high plasticity clay (e).

phases (out of the six measured) are exemplified in Fig. 4e for the sample 'optimum' of high plasticity clay.

The first drying phase of all samples is very similar as observed in Fig. 3a,b. In the case of the scanning wetting phases and scanning drying phases, some differences can be observed among samples (Fig. 3c-f). The differences observed in Figs. 2 and 3 could indicate that there might be an effect of the compaction conditions on the shape of the SWRC-e_w. As SWRC-e_w exclude volume changes, the effect would have to be related to different fabrics. It has been demonstrated that compacting soil at different water content but with the same vertical stress leads to different pore-size distributions [35]. Soil compacted at the same water content but with different energy has been observed to present different inter-aggregate porosity while the intra-aggregate porosity remains unchanged [13,22,23,29,36]. It is possible that this could have an effect of the shape of the SWRCs-e_w. However, this possible influence of the compaction conditions is of similar magnitude to the variability within the experimental results. Therefore, it would not be justified to introduce another level of complexity to the proposed model.

Regarding the evolution of the SWRC-e_w with drying wetting cycles, it was observed that the decrease in the initial water ratio was more accentuated between the first and the second drying phase (decrease of up to 0.17), therefore, supporting the need to differentiate the primary drying phase from the scanning drying phases (Fig. 4a,b). The decrease of the final water ratio was of up to 0.04 and no change was observed in most cases (Fig. 4c,d). The change of the final water ratio was smaller than the change in the initial water ratio, showing that a smaller variation of water ratio is needed to produce the same change in suction with increasing number of cycles.

It is commonly assumed that the slope of the scanning branches of the SWRC remain the same independently of the drying and wetting processes the soil may have undergone. Here, the possibility that the SWRCs change with drying-wetting cycling was investigated by studying the fitting parameters b_w and b_d for each sample and for each cycle while the other parameters remained constant and equal to the values reported

in Table 3. The evolution of parameters b_w and b_d of each sample is reported in Fig. 5. The parameter b_w, that controls the shape of the wetting branches of the SWRC, decreases with increasing number of cycles for both clays. Samples compacted on the wet-side ('dense' and 'wet') appear to present a higher value of b_w than the samples compacted on the dry-side ('dry' and 'loose') for HP clay. The same sequence is not as clear in the samples of VHP clay. The value of b_d, that controls the shape of the drying scan branches of the SWRC, slightly decreases with increasing number of cycles for the VHP clay, but the value of this parameter remains constant within a range of variability between 1.1 and 1.3. No effect of the compaction conditions on b_d is evident in Fig. 5. Thus, there might be an effect of the compaction conditions on the slope of the wetting branches of the SWRC, possibly some evidence for a 'fatigue' or 'deterioration' effect of the cycling on the hydraulic properties of the soil. However, for the drying curves the slope of the scanning curves is unaffected by either compaction conditions or cycling.

The proposed method of predicting SWRCs using Equations (1) to (3) produces closed-loops when suction is varied within a well-defined range. However, in the performed experiments, some variability was observed in the bounds of the interval of suction variation. The initial suction of the drying phase varied between 0.8 and 2.2 MPa, while the final suction varied between 69.6 and 105.6 MPa. This variability results in changes in the respective predicted initial and final water ratio of each drying SWRC-e_w thus capturing the changes observed in Fig. 4a-d caused by the moisture cycling, even if the fitting parameter b_w is assumed constant with drying-wetting cycles.

The main difference between the tested clays is the clay content, which leads to different liquid limits. The VHP clay presents higher clay fraction and higher liquid limit that results in a higher plasticity index. A finer soil results in more smaller pores which affect the water retention properties of the soil. It is generally observed that for soil with higher fine content and higher plasticity, the SWRCs tend to move towards higher air-entry values and hence towards higher suctions. This was observed experimentally in the present study as the SWRCs of the VHP clay plot at slightly higher suctions than the SWRCs of the HP clay (Fig. 3).

Soil shrink-swell curves

Modelling soil shrink-swell curves

In order to estimate the soil–water retention curves (SWRCs) accounting for the volume changes, the generic SWRCs mentioned above have to be combined with the soil shrink-swell curves (SSSCs) described in the present section. Fig. 6 presents the SSSCs of phases 'drying 1', 'wetting 1' and 'drying 2' of the sample 'dense' of VHP clay to illustrate typical SSSCs and the fitting of the model.

The shrinkage components observed in the SSSCs of this study are characterized by three different phases (from wet to dry; Fig. 6): (i) proportional shrinkage, when the variation of pore volume and water volume is equal; (ii) residual shrinkage, when the decrease in the volume of pores is smaller than the volume of water loss; and (iii) zero shrinkage, when there is no further volume change with decreasing water content [37,38].

The adopted SSSC was defined in terms of void ratio (e) as a function of water ratio (e_w) using Eq. (4), where e_{min} is the minimum void ratio (below the apparent shrinkage limit), and c and d are fitting parameters. The SSSCs were fitted for each individual phase of each tested sample. If the equation predicted a water ratio such that $\frac{de_w}{de} > 1$ (an unfeasible case), the void ratio was imposed to be greater than or equal to the water ratio ($e \geq e_w$) and the variation of void ratio was imposed to be equal to the variation of water ratio estimated using the generic SWRC-e_w ($\Delta e = \Delta e_w$). These conditions were necessary so that the degree of saturation could not exceed 1 and so that the estimated degree of saturation could not increase with increasing suction. This condition is necessary for the estimation of SWRCs in terms of degree of saturation, i.e., accounting for volume changes during drying-wetting cycles, by combining the generic SWRC with the estimated SSSC. This will be explored in the section that follows.

$$e = e_{min} + (e_w + c)^d \tag{4}$$

In Fig. 6, the first drying phase starts from a state close to saturation and the variation of water ratio is equal to the variation of void ratio

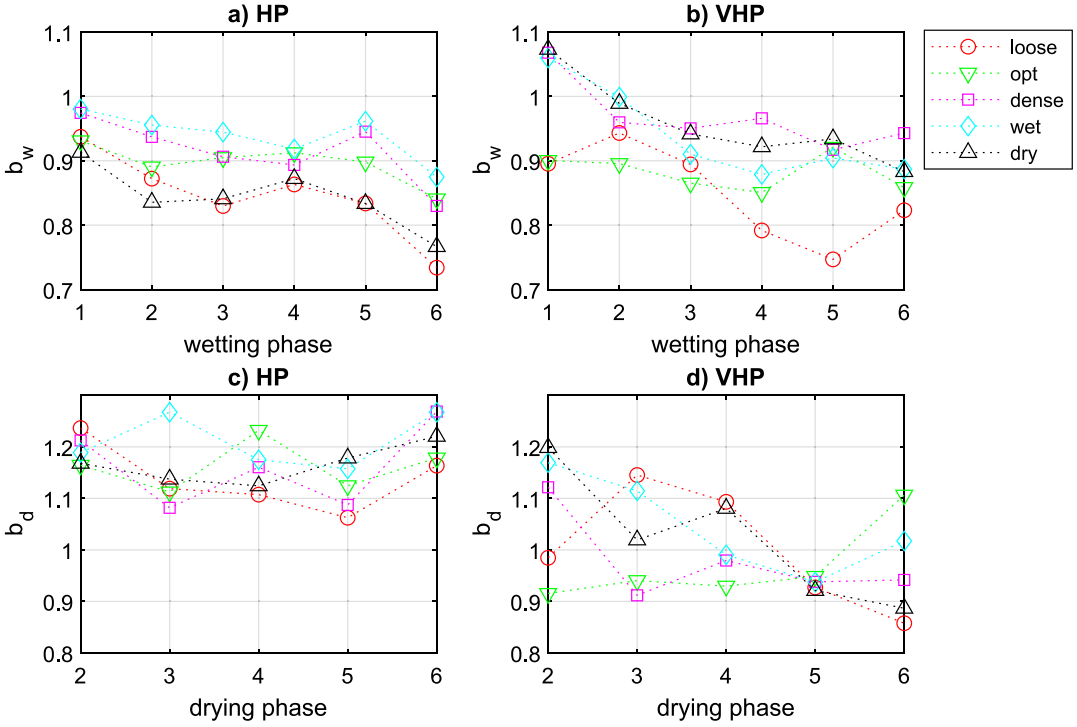

Fig. 5. Evolution of the fitting parameters b_w and b_d of Equations (2) and (3) for high plasticity (HP) and very high plasticity (VHP) clay.

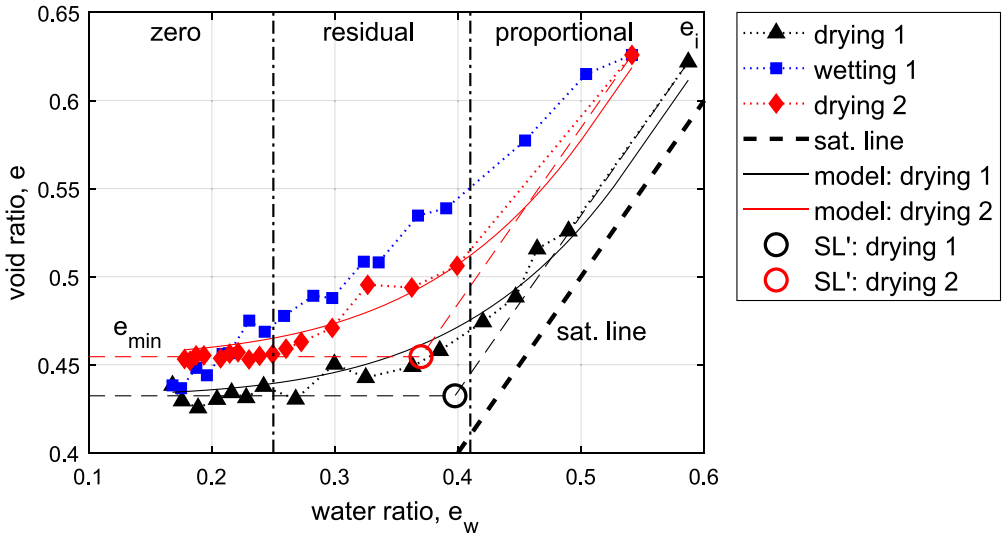

Fig. 6. Soil shrink-swell curves of the sample "dense" of very high plasticity clay. Identification of the zero, residual and proportional shrinkage phases. Constructions to obtain the apparent shrinkage limit (SL') of the phases 'drying 1' and 'drying 2' using the initial void ratio (e_i) and the minimum void ratio upon drying (e_{min}). Fitted SSSC model for the drying phases.

maintaining this level of saturation ($\Delta e = \Delta e_w$). When the sample starts to desaturate, entering the residual shrinkage phase, the SSSCs is given by Eq. (4) and the void ratio tends to e_{min}. For the second drying phase, when the proportional shrinkage phase is parallel to the saturation line, $\Delta e = \Delta e_w$ is also imposed.

Fitting of soil shrink-swell curves and discussion

The model described by Eq. (4) was fitted to each individual phase of the tested samples. Both fitting parameters (c and d) influence the slope and the position of the apparent shrinkage limit. Therefore, a sensitivity analysis was performed to attempt to simplify the model fitting, even though it was clear that the parameter c influences more significatively the slope of the proportional shrinkage phase, while changing parameter d influences mostly the position of the apparent shrinkage limit.

The sensitivity analysis consisted of perturbing each fitting parameter by one standard deviation (considering the fitting parameters of all phases and samples of both clays). The sensitivity analysis showed that the model is equally sensitive to both fitting parameters, i.e., the difference between the estimated void ratio and the actual void ratio was within the same interval. However, disturbing the parameter c led to deviations in the estimation of the void ratio that showed a trend that appeared to be exponential with increasing water ratio. As the accurate estimation of the void ratio for a high water content, or low suction, are critical for an accurate estimation of SWRCs, the parameter c was selected as a parameter that could vary with drying-wetting cycles. Therefore, all the phases of the samples of a given clay present a constant parameter d that was adopted to be the average of all phases: $d = 5.85$ for the HP and $d = 5.29$ for the VHP clay (respective standard deviation of 2.42 and 1.14).

A second fitting was performed adopting the parameter d values previously mentioned. The fitting parameter c is presented in Fig. 7, showing an increase with increasing number of cycles in both drying and wetting phases. The increase in the parameter c represents a more rapid transition from proportional shrinkage to residual shrinkage and lower apparent shrinkage limits (water content below which no volume changes are observed). The parameter c is lower in the drying phases than in the wetting phases for the HP clay (Fig. 7e,f), revealing that the evolution of the SSSCs results from a combined effect of wetting SSSCs that have a rapid transition from zero-shrinkage to proportional shrinkage and drying SSSCs with progressively lower apparent shrinkage limits (as observed in the example of Fig. 6).

The compaction conditions appear to influence the values of parameter c because its value is usually higher for the 'loose' samples than for the 'dense' samples, and the same value is usually higher for 'dry' samples than for the 'wet' samples. However, differences among samples were not observed to be consistent throughout all the performed cycles.

The volume changes exhibited by specimens prepared at different compaction conditions are shown in terms of water ratio versus void ratio in Fig. 8. The phases identifiable in the drying phases of the SSSCs are the proportional shrinkage, the residual shrinkage, and the zero shrinkage [38]. During the drying phases the samples showed a decrease in the void ratio (e) down to a certain limit with decreasing water ratio. Then, the volume change is partially or totally reversed upon wetting. Samples compacted at different conditions present a different response to drying and wetting phases which can be quantified by the slope of the proportional shrinkage phase of the SSSC, the minimum void ratio reached upon drying, the apparent shrinkage limit (water content beyond which no further volume change occurs upon drying), and the evolution of the previous properties with increasing number of cycles.

The initial and final void ratio of each drying phase is presented in Fig. 9. The initial void ratio tends to decrease or remain constant with increasing number of cycles, even though the initial water ratio decreases (Fig. 4a,b). The decrease in the initial water ratio for a constant value of initial void ratio with increasing number of cycles translates in SSSCs becoming progressively further away from the saturation line (Fig. 8) and lower degrees of saturation at the beginning of each drying phase. The propagation of the SSSCs towards lower degrees of saturations with increasing number of cycles has been also observed by Tripathy et al. [19] and Estabragh et al. [21]. No explanation for this phenomenon has been proposed by these authors, but it will relate to fabric changes in the soil.

The final void ratio evolution with increasing number of cycles depends on the compaction conditions (Fig. 9 c,d). The samples compacted at maximum Proctor density ('wet', 'optimum' and 'dry') do not present changes with increasing number of cycles. However, 'dense' samples present a progressive increase in the final void ratio upon drying, which the 'loose' samples present a progressive decrease in the final void ratio. The effect of the compaction density observed is in agreement with Nowamooz and Masrouri [20] who observed that a denser compacted sample presented accumulated swelling while a 'loose' sample accumulated shrinkage after one cycle. It was observed that the 'dense' samples of both clays formed cracks on the surface of the sample, which

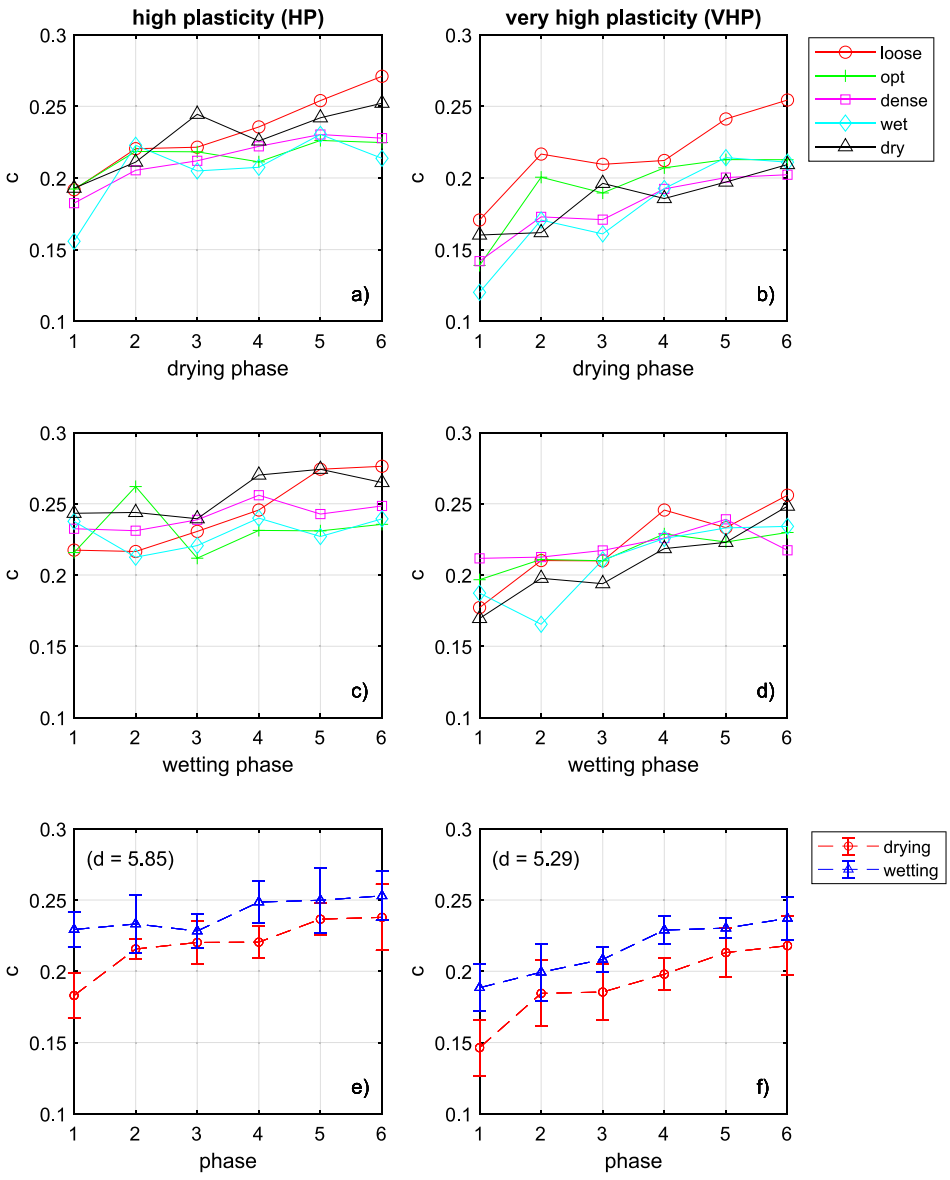

Fig. 7. Evolution of the fitting parameter c for drying (a, b) and wetting (c, d) phases of each sample of high plasticity (HP, left) and very high plasticity (VHP, right) clay. The average and standard deviation, represented by error bars, of drying and wetting phases of high and very high plasticity clay (e, f).

can explain the observed increase in the final void ratio. The 'loose' samples presented an increase in the final void ratio with cycling, which may be due to a rearrangement of the clay particles within the soil aggregates as a result of the increase in suction during drying. The continuous evolution of the final void ratio shows evidence of fatigue behaviour, in which the change occurs with repeated cycles with decreasing intensity [19,21,39].

In the case of the 'loose' samples, the decreasing final water ratio is compensated by a decreasing final void ratio that leads to no change in the final degree of saturation. In all the remaining samples, the decrease of the final water ratio with increasing number of cycles leads to a decrease of the final degree of saturation because the final void ratio remains constant or decreases. This observation is in agreement with previous studies where this evolution has been reported as the shift in the SWRCs towards lower suctions with increasing number of cycles [6,40], that is, for the same suction, a decrease in the degree of saturation is observed due to moisture cycling. This decrease in degree of saturation can be caused by an increase of the void ratio or/and a decrease of the water ratio, as observed in the present study.

The apparent shrinkage limit can be determined by the intercept of the saturation line ($S_r = 1$) with the horizontal line passing through the minimum void ratio upon drying, representing the transition from a saturated to an unsaturated state, beyond which no further volume changes occur (Fig. 6). However, in the present study, the samples start from an unsaturated state, and the transition from the proportional to the zero-shrinkage phase can be referred to as an apparent shrinkage limit [18]. The method of determining the apparent shrinkage limit used here is based on the observation reported in Tripathy et al. [19] that shrinkage curves present proportional shrinkage phases parallel to the saturation line ($S_r = 1$) when represented in terms of gravimetric water content versus void ratio. Therefore, a line tangent to the proportional shrinkage phase (parallel to the saturation line $S_r = 1$, for which $\Delta e = \Delta e_w$) is used to intercept the horizontal line through the minimum void ratio upon drying (Fig. 6). Therefore, the apparent shrinkage limit in terms of gravimetric water content (SL') was defined by Eq. (5), where e_{ps} and $e_{w,ps}$ are any point in the proportional phase of the shrinkage curve. It is worth noting that the conversion between gravimetric water content (w) and water ratio (e_w) is based on the relation $e_w = w \bullet G_s$, where G_s is the soil specific gravity.

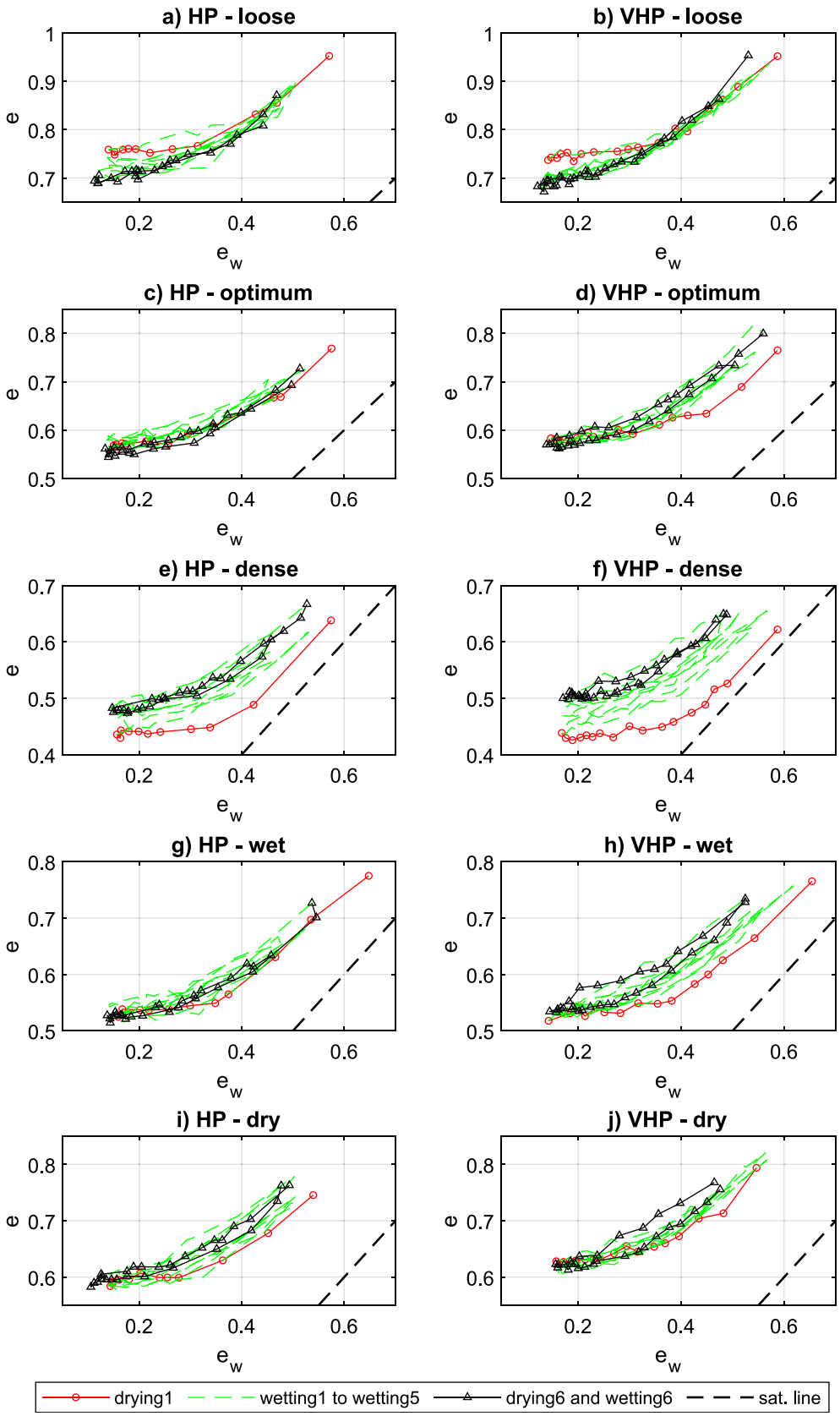

Fig. 8. Soil shrink-swell curves in terms of void ratio (e) versus water ratio (e_w) for samples of High Plasticity (HP) clay (left) and Very High Plasticity (VHP) clay (right) compacted at different conditions subjected to six cycles of drying and wetting. The phases 'drying 1′ to 'drying 2′ (initial phases) are represented in red, the phases 'wetting 2′ to 'wetting 5′ (intermediate cycles) are represented in green, and the phases dry 6 and wet 6 (final cycle) are presented in black, and the saturation line ($S_r = 1$) is the dashed black line. (For interpretation of the references to colour in this figure legend, the reader is referred to the web version of this article.)

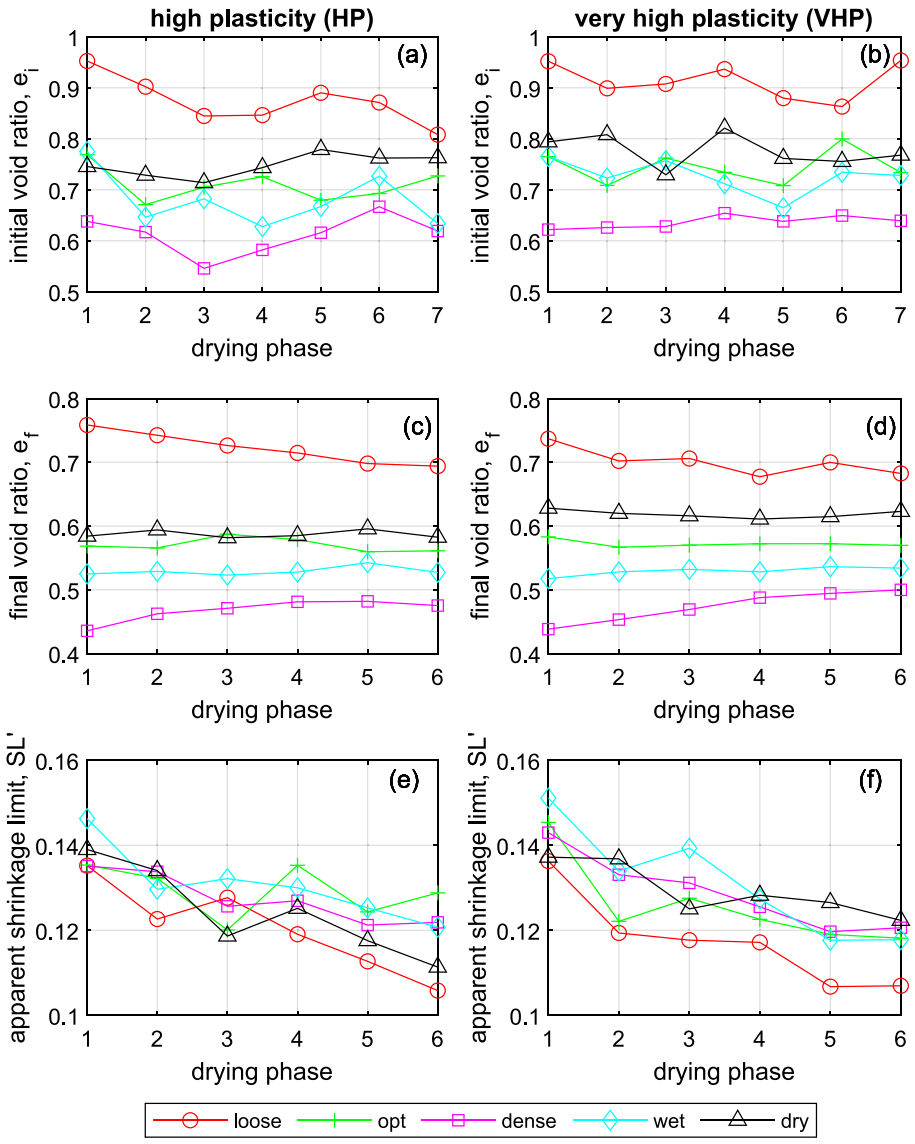

Fig. 9. Evolution of the initial and final void ratio, respectively e_i and e_f, and the apparent shrinkage limit (gravimetric water content) of each drying phase of samples of High Plasticity (HP) clay (left) and Very High Plasticity (VHP) clay (right) compacted at different conditions.

$$SL' = (e_{min} - (e_{ps} - e_{w,ps}))/G_s \quad (5)$$

In the present study, the proportional shrinkage phase is not complete, but all cycles reach the proportional shrinkage phase, as identified in Fig. 6 and observed in all samples in Fig. 8. Therefore, e_{ps} and $e_{w,ps}$ can be assumed equal to e_i and $e_{w,i}$ (initial state of each drying phase), respectively.

The apparent shrinkage limit depends on the compaction conditions as the looser samples present the lowest apparent shrinkage limit (Fig. 9e,f). Furthermore, the apparent shrinkage limit decreases with increasing number of cycles in all tested samples. The propagation of the SSSC further away from the saturation line and/or a decrease of e_{min} results in a decrease of the apparent shrinkage limit (Fig. 8). The 'loose' samples present no propagation of the proportional shrinkage phase but the minimum void ratio upon drying decreases (Fig. 8a,b), for which the apparent shrinkage limit decreases (Fig. 9e,f). The 'dense' samples present a propagation of the proportional shrinkage phase towards lower degrees of saturation, but the minimum void ratio upon drying increases (Fig. 8e,f), for which the decrease of the apparent shrinkage limit with cycling is less evident than in looser samples (Fig. 9e,f).

The apparent shrinkage limit of the VHP clay is slightly higher than for the HP clay for samples compacted at the same conditions. This can result from the fact that the VHP clay samples were compacted at a lower void ratio than the HP clay samples. The different density results in SSSCs that are closer to the saturation line, as observed in Fig. 7. No significant changes in the final void ratio were observed between samples compacted at the same condition for both clays (Fig, 8c,d).

Soil-water retention curves dependent on soil volume

Modelling of soil–water retention curves

The SWRC-S_r considering the volume changes described in terms of degree of saturation was obtained by combining the generic SWRC-e_w with the SSSCs. The known initial conditions are suction, water ratio and void ratio. Then, given a known variation of water ratio, Eqs. 1–3 were solved to estimate suction and Eq. (4) was solved to obtain the void ratio. The degree of saturation (S_r) is then given by Eq. (6).

$$S_r = \frac{e_w}{e} \quad (6)$$

When determining the predicted primary drying SWRC, it is

observed that the known initial water ratio may plot slightly below or above the fitted line (Fig. 3a,b), because of a small deviation between the experimental data and the fitted SWRCs and possible effects that the compaction still shows on the SWRC for starting at water ratios close to the boundary between capillary and adsorptive regime. Hence, it is assumed that the initial state of the soil (suction and water ratio) is on a scan drying SWRC before it intersects the primary drying SWRC. If the measured suction at compaction is lower than the predicted value, then the SWRC is characterized by the slope of the scanning drying SWRC (Eq. (3), assuming $s_{i-1} = 80MPa$) until the scanning drying SWRC encounters the primary drying SWRC (Eq. (1). If the measured suction is higher than the predicted value, as in the case of sample 'wet' of the HP clay (as we observed to be in the capillary regime according to the relationships of Chen and Lu [31]), then the change in suction was imposed to be linear in the semi-logarithm scale between the first and the second measured suction values so that impossible estimations are not obtained, such as an increase in the degree of saturation during a drying process.

Experimental soil–water retention curves in terms of degree of saturation

The measured SWRC-S_r cycles are presented in Fig. 10. Lines with circles show the first drying phase, with subsequent curves shown as dotted curves and the final dry-wet cycle shown as lines with triangles. All samples present slightly different shape and different changes with progressive cycling depending on the compaction conditions. Differences are also present when comparing samples of different clays compacted at same conditions, as the shift with increasing number of cycles is greater in the VHP plasticity samples.

Samples compacted at lower void ratio present higher suction for the same degree of saturation. The cycling results in lower suctions for the same degree of saturation, but the denser samples still preserve the higher levels of suction for the same degree of saturation when compared with other compaction conditions. Nonetheless, the shift in the SWRC-Sr of the 'dense' samples is the greatest among the tested conditions. Soil compacted at higher water content presented higher suction values during the first drying phase and after drying-wetting cycling (for a given degree of saturation).

Therefore, soil compacted on the wet-side and at a denser state holds higher values of suction even after being subjected to drying-wetting cycles, which results in a greater contribution of the suction to the soil shear strength in unsaturated conditions. These compaction conditions could be the ideal ones in the construction of embankments. However, it should be taken into account that the dense state is the one that presents the greatest overall decrease in suction as a consequence of moisture cycling, so while the suction remains higher than for other cases, it may show a more significant loss in performance compared to its initial state.

Estimation of soil–water retention curves accounting for volume changes

The SWRC-S_r was estimated based on the simulations obtained using the generic SWRC-e_w and the SSSCs (void ratio vs water ratio) described in the previous sections. The SWRC-S_r is then the representation of the estimated degree of saturation versus the estimated suction. Fig. 11 presents the estimation of suction, void ratio and degree of saturation of the samples 'loose', 'optimum' and 'dense' of high plasticity clay as an example of simulations produced by the presented semi-empirical model.

The comparison between the measured and the calculated values of suction, void ratio and degree of saturation are presented in Fig. 12. A line with a slope of 1 and intercept 0, referred to as 1:1 line, is presented to support in the assessment of the quality of the calculation method. It is visible that the estimated values plot close to the 1:1 line for all cases. The calculated suction is the parameter that presents the greatest deviation from the measured values, especially for low values of suction. Nonetheless, the estimated deviations are approximately of 1 MPa for the lowest measured suction values. A linear regression of the plotted data points is presented above each of the subplots. The slope of close to 1, varying between 0.973 and 1.068, and the intercept is close to zero, being always lower than 0.181. This indicates the excellent quality of the fitting.

The SWRC-e_w does not present significant differences between different compaction conditions. Moreover, the simulated SWRC-e_w change with progressive drying-wetting cycles is solely due to variability in the reversal point because the model produced closed loops and does not allow fatigue behaviour. The three different curves (primary drying, scanning wetting and scanning drying) are properly estimated. The SSSCs presented in Fig. 11 correspond to the fitted model, for which the R^2 is not observed to change with increasing number of cycles.

The estimated SWRC-S_r presents agreement with the experimental data (Fig. 11c,f,i). The 'dense' and 'loose' samples present opposing behaviour represented by the propagation of the SSSC with increasing number of cycles, which results in different SWRC-S_r. The sample 'optimum' represents an intermediate behaviour of the evolution of the SSSCs.

The 'dense' sample (Fig. 11i) presents the most evident change of the SWRC-S_r with increasing number of cycles. The SSSC of the 'dense' sample propagates away from the saturation line in the proportional shrinkage phase as the void ratio increases for the same water ratio that leads to a decrease of the degree of saturation at low suctions visible in the SWRC- S_r. In the zero-shrinkage phase, the e_{min} tends to increase with increasing cycling, combined with no evolution of the SWRC-e_w, that leads to a decrease of the degree of saturation in the high suction range as well. In this way, the SWRCs-S_r propagates entirely towards lower degrees of saturation.

In the 'loose' sample (Fig. 9c), a difference can be observed between the primary drying and the scanning drying phases in terms of degree of saturation, but the scanning drying phases do not evolve significantly with progressive cycling. The proportional shrinkage phase does not change with cycling, but the zero-shrinkage phase propagates towards lower e_{min} values (Fig. 11b). The model simulates a slight increase in the degree of saturation in the higher suction range with cycling as a consequence of the decrease in void ratio in the zero-shrinkage phase. However, the change in the SWRC-S_r is not in agreement with the experimental data because the primary and scanning drying experimental data overlap in the high suction range. Nonetheless, an actual decrease of the final water ratio was observed (Fig. 4c), which combined with a decrease of the e_{min} could result in no change of the SWRC-S_r.

The proposed model was therefore capable of estimating the SWRCs considering the effect of volume changes using a single generic SWRC model in terms of water ratio. The advantage of the presented strategy lies in the fact that SSSCs are easier to measure than SWRCs. Measuring the SWRCs requires performing measurements of suction, which often constitutes a challenge [41,42]. However, measuring SSSCs only requires the monitoring of volume and weight changes in a soil sample, which can be done using a calliper and a balance, respectively, as in the present study.

It has to be recognised that in full scale embankments, the water flux is controlled by both the hydraulic properties of the soil and by the presence of fissures and cracks [43]. The cracks observed in the field are of greater dimensions than the ones observed in the present study and would influence the influx of water through different mechanisms [44,45]. The SWRCs obtained in the present study reflect the behaviour of the soil material itself, not the large-scale fabric.

Discussion on the prediction of soil–water retention curves

As the generic SWRC-e_w was used to represent the hydraulic behaviour of all the samples independently of the compaction conditions, it would be expected that the primary drying SWRC-e_w could represent an upper boundary to all possible states of the soil. The SWRCs

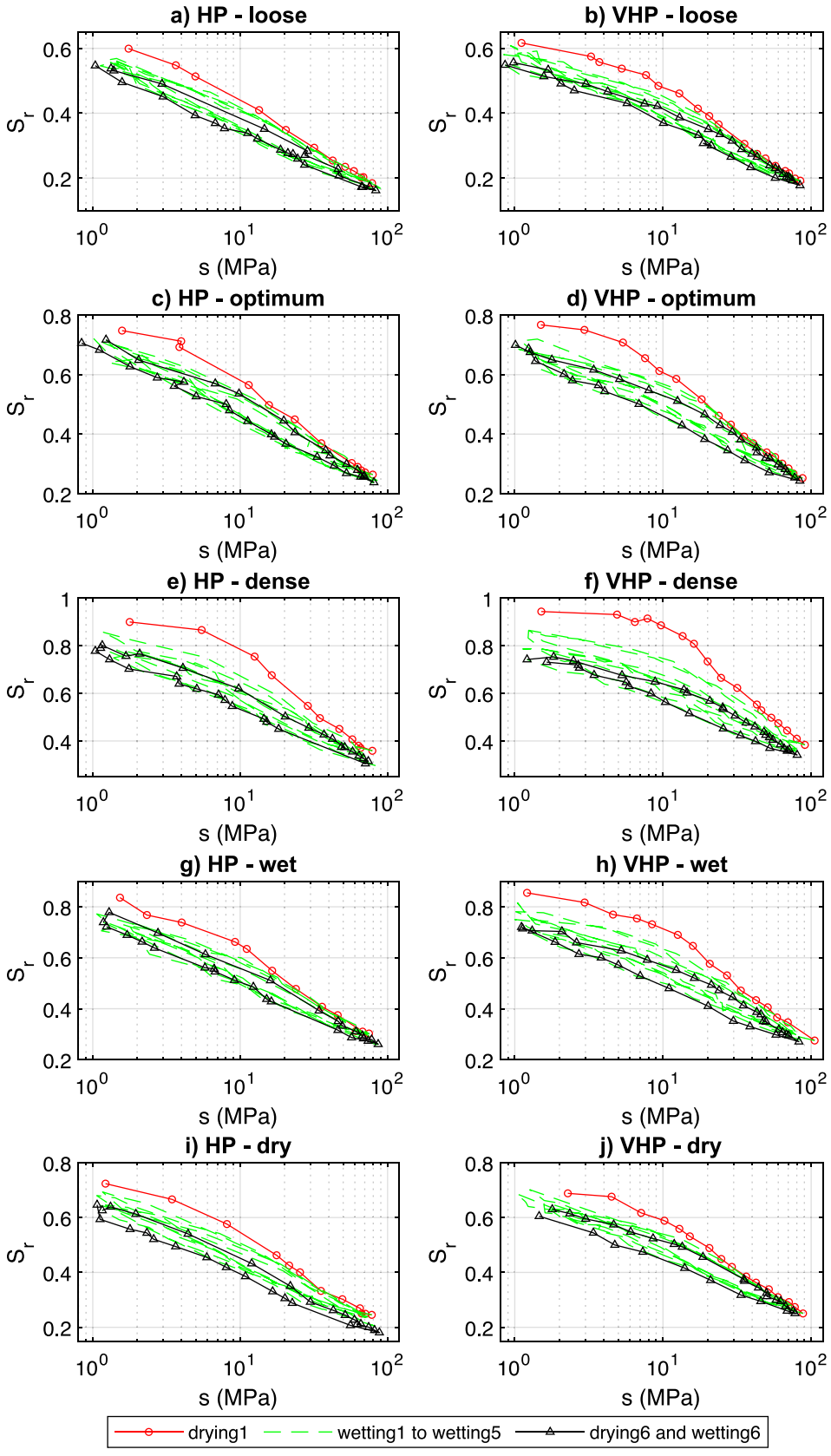

Fig. 10. SWRCs in terms of degree of saturation (S_r) versus suction (s) for samples of High Plasticity (HP) clay (left) and Very High Plasticity (VHP) clay (right) compacted at different conditions subjected to six cycles of drying and wetting. The phases 'drying 1′ to 'drying 2′ (initial phases) are represented in red, the phases 'wetting 2′ to 'wetting 5′ (intermediate cycles) are represented in green, and the phases dry 6 and wet 6 (final cycle) are presented in black. (For interpretation of the references to colour in this figure legend, the reader is referred to the web version of this article.)

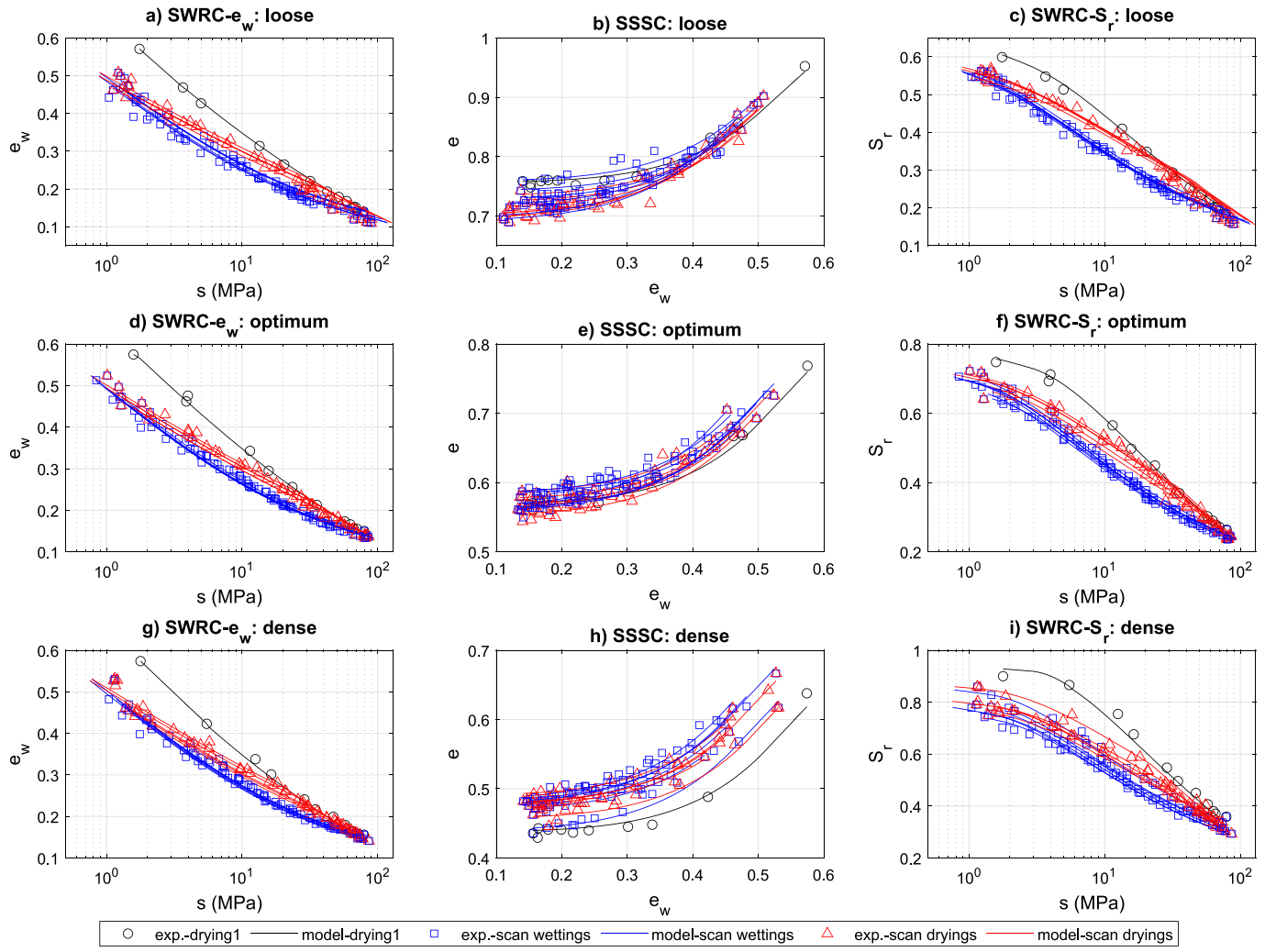

Fig. 11. Simulated SWRCs in terms of water ratio (e_w), fitted SSSCs in terms of water ratio versus void ratio (e), and estimated SWRCs in terms of degree of saturation (S_r), at three different compaction conditions ('loose', 'optimum' and 'dense') of the high plasticity (HP) clay.

and SSSCs were represented in the suction-void ratio-water ratio space in Fig. 13. The experimental data points of the first drying phases of all the samples are on the surface defined by the primary drying SWRC-e_w, as well as the portion of the scanning drying curves at suction values above approximately 30 MPa (see also Fig. 3).

A second upper boundary condition was also represented in Fig. 13 and it establishes that the water ratio has to be always equal or lower than the void ratio ($e_w \leq e$). If the soil is saturated, i.e., $S_r = 1$, then $e_w = e$ and this boundary can be referred as the saturation surface. The intercept between both upper boundaries is here referred to as the saturation line (dark blue line in Fig. 13). The first drying phase of all samples follow paths parallel to the saturation line as already observed in Fig. 8. This saturation line represents the fact that the air-entry value is observed to increase with decreasing void ratio as a consequence of the decrease of the pores' sizes.

Both the primary drying condition and the saturation line act independently in the estimation of the SWRC-S_r, for which first drying is represented in Fig. 14 alongside the experimental measurements. For example, the starting point can be over the saturation surface, but at a lower suction than the saturation line (Fig. 13). In this case, the suction change might be defined by the slope of the scanning drying SWRC-e_w until encountering the saturation line, after which the suction change might be determined by the primary drying surface. Nonetheless, even after encountering the saturation line, the degree of saturation can remain constant and the predicted SWRC will not change until air starts to enter the soil voids. This change in the slope of the SSSC, which represents a slowing down of the volumetric deformations upon drying, coincides with the change in the slope of the SWRC-S_r (Fig. 14). The air-entry value identified in the SWRC-S_r is therefore associated with the apparent shrinkage limit.

Conclusions

Compacted samples of high and very high plasticity London clay were prepared with different water content and dry density to study the effect of the volumetric deformations on the Soil-Water Retention Curves (SWRCs) with moisture cycles. The samples were subjected to six drying-wetting cycles between 1 and 80 MPa, while water content, total suction and volume changes were recorded.

It was found that within the adsorptive region a single generic SWRC in terms of water ratio (SWRC-e_w), that is independent of the compaction conditions, can be identified. This single generic SWRC model, composed of a primary drying curve, scanning wetting and scanning drying phases, was fitted to the experimental data. The model was able to estimate the suction over the six drying-wetting cycles without propagation of error. Moreover, the primary drying curve was identified as an upper boundary condition to all possible soil states in terms of suction and water content independently of the void ratio of the soil.

The Soil Shrink-Swell Curves (SSSCs) were observed to depend on the compaction conditions. The SSSCs of denser samples, and samples

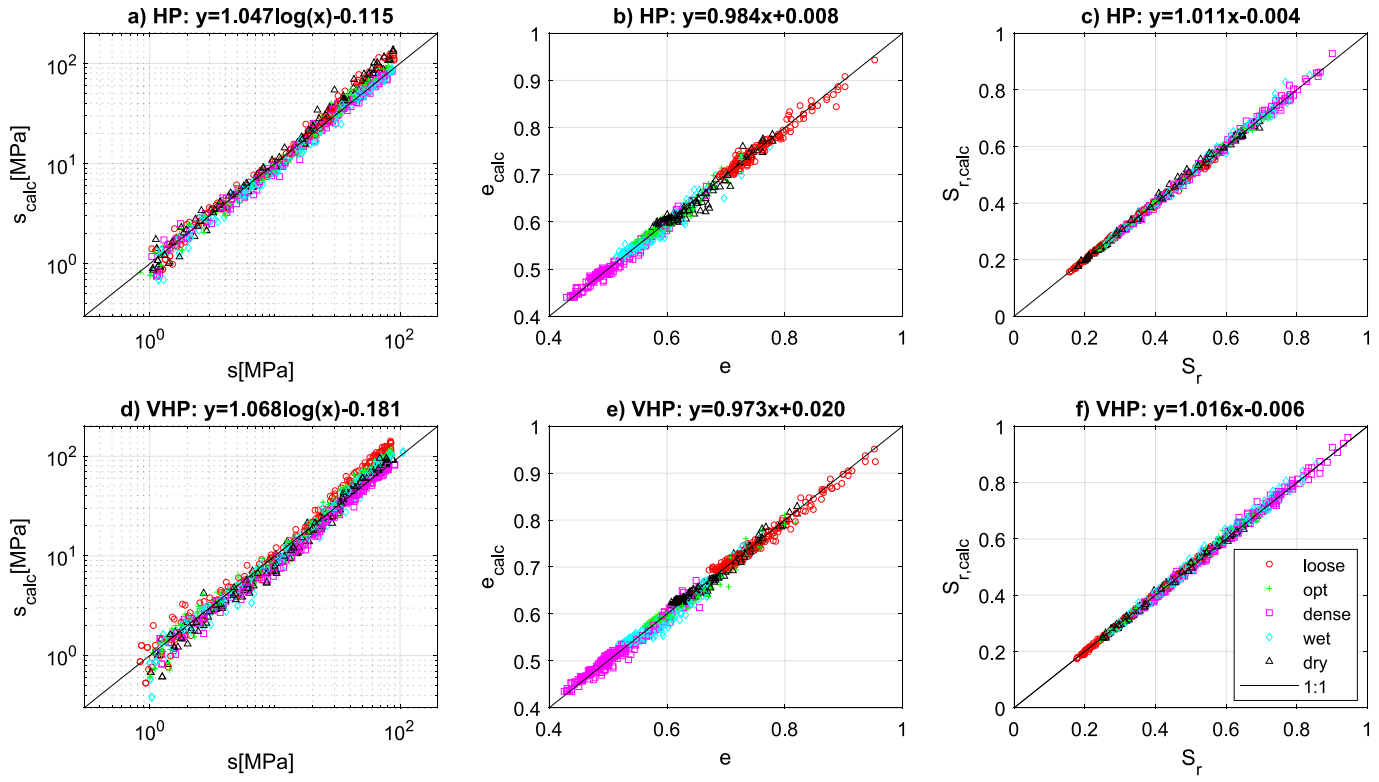

Fig. 12. Comparison of the measured values with the calculated values of: (a, d) suction (s); (b, e) void ratio (e); and (c, f) degree of saturation (S_r), for the high plasticity (HP) and very high plasticity (VHP) clays.

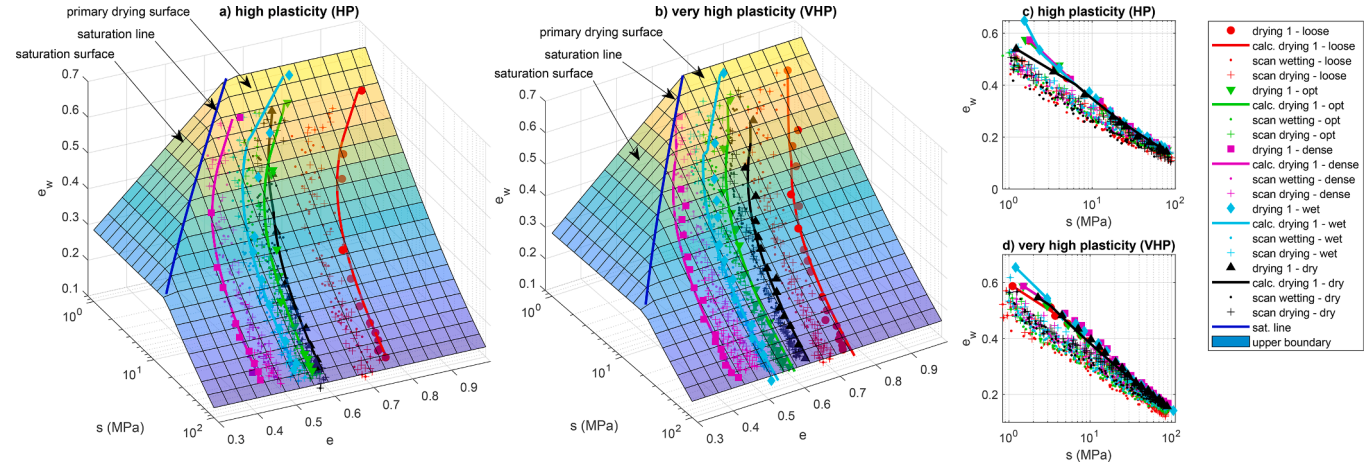

Fig. 13. Upper boundaries of the soil–water retention curves of (a,c) high plasticity (HP), and (b,d) very high plasticity (VHP) clay, represented in terms of total suction (s), void ratio (e), and water ratio (e_w). The primary drying experimental data and respective estimation of the SWRC is presented (identified by 'dry1′ and 'calc.dry' in the legend). The scan drying and wetting experimental measurements are presented.

compacted at higher degree of saturation, present lower apparent shrinkage limit values, steeper proportional shrinkage phases and higher minimum void ratios upon drying. The evolution of the SSSCs with drying-wetting cycling also depends on the compaction conditions. Looser samples present a more evident change in the slope of the proportional shrinkage phase and apparent shrinkage limit, even though these tend to stabilize with increasing number of cycles in all samples. The minimum void ratio reached upon drying evolves with cycling depending on the compaction conditions: 'dense' samples present an increase in the void ratio, while the 'loose' samples present a decrease in the void ratio. Samples compacted at Proctor optimum do not present a change in the minimum void ratio reached upon drying.

The SWRCs in terms of degree of saturation (SWRC-S_r), which consider the volume changes occurring during the drying-wetting cycles, depend on the compaction conditions. It was observed that soil compacted at a denser state and on the wet-side holds higher suction even after being subjected to drying-wetting cycles compared to the remaining tested conditions, which indicates these could be the ideal condition for the compaction of embankments in which suction can have a higher impact on the shear strength of the soil. However, these were the conditions in which a greater overall decrease in suction was observed as a consequence of moisture cycling (even though overall suctions remained higher) which could indicate that Earthworks compacted at those conditions may be more susceptible to greater

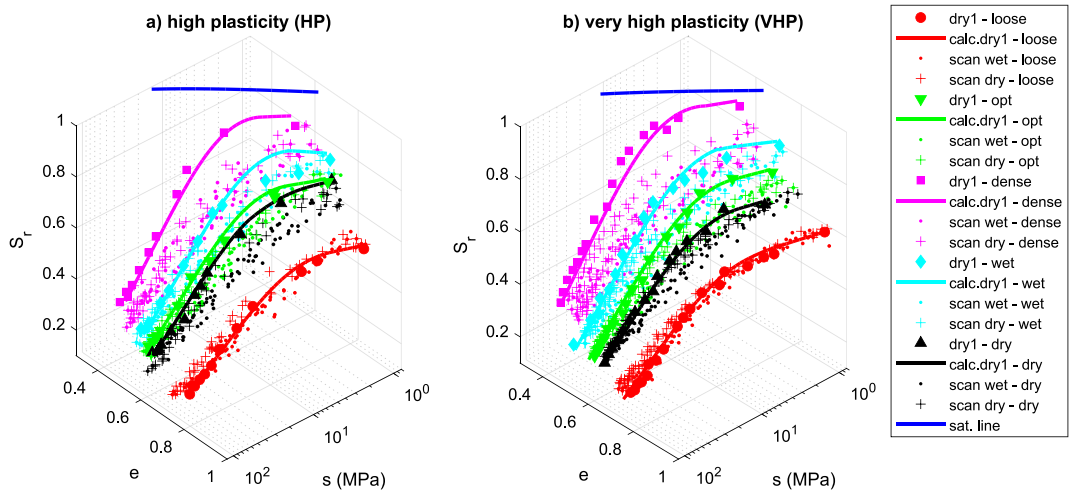

Fig. 14. Experimental soil–water retention curves of (a) high plasticity (HP), and (b) very high plasticity (VHP) clay, represented in terms of total suction (s), void ratio (e), and degree of saturation (S_r). The predicted SWRC-Sr of the first drying phase and the saturation line are highlighted.

deterioration relative to the initial state.

The SWRC-S_r were predicted from combining a generic SWRC-e_w with the SSSC of the sample of interest. This method does not require extensive measurements of SWRCs but relies more on simpler SSSCs that are easier to determine. The method constitutes a tool to determine SWRCs and their evolution for soil exposed to weather cycles. The estimated SWRCs can be used in the modelling of the pore-water pressure regime on active clays subjected to cycles of evaporation and rainfall, such as embankments and cuttings. In this way, the deterioration of the hydraulic properties of the soil can be better represented in geotechnical models used to simulate the performance of earthworks.

CRediT authorship contribution statement

Ana Sofia Dias: Methodology, Formal analysis, Data curation, Writing – original draft, Writing – review & editing, Conceptualization, Investigation. **Paul N. Hughes:** Writing – original draft, Supervision, Conceptualization, Resources, Writing – review & editing. **David G. Toll:** Supervision, Writing – original draft, Writing – review & editing, Conceptualization, Resources. **Stephanie Glendinning:** Supervision, Funding acquisition, Conceptualization.

Declaration of Competing Interest

The authors declare that they have no known competing financial interests or personal relationships that could have appeared to influence the work reported in this paper.

Data availability

The data and supplementary documents are available at: http://doi.org/10.15128/r2jm214p22c.

Acknowledgements

The work presented is an output of the ACHILLES programme grant (programme grant number EP/R034575/1) funded by the UK Engineering and Physical Sciences Research Council (EPSRC). The authors would like to acknowledge Stephen Richardson and Kevan Longley at Durham University for their assistance with the laboratory testing.

References

[1] Rail N. Annual expenditure 2016–17. Milton Keynes, UK: Network Rail; 2017.
[2] Rail N. Annual expenditure 2017–18. Milton Keynes, UK: Network Rail; 2018.
[3] Hughes PN, Glendinning S, Mendes J, Parkin G, Toll DG, Gallipoli D, et al. Full-scale testing to assess climate effects on embankments. Proc Inst Civ Eng Bridg Eng 2009;162(2):67–79.
[4] Dijkstra TA, Dixon N. Climate change and slope stability in the UK: challenges and approaches Subscribe. Q J Eng Geol Hydrogeol 2010;43(4):371–85.
[5] Briggs KM, Loveridge FA, Glendinning S. Failures in transport infrastructure embankments. Eng Geol 2017;219:107–17. https://doi.org/10.1016/j.enggeo.2016.07.016.
[6] Stirling RA, Toll DG, Glendinning S, Helm PR, Yildiz A, Hughes PN, et al. Weather-driven deterioration processes affecting the performance of embankment slopes. Géotechnique 2021;71(11):957–69.
[7] Fredlund DG. The 1999 R.M. Hardy Lecture: The implementation of unsaturated soil mechanics into geotechnical engineering. Can Geotech J 2000;37:963–86. https://doi.org/10.1139/t00-026.
[8] Postill H, Helm PR, Dixon N, El-Hamalawi A, Glendinning S, Take WA. Strength parameter selection framework for evaluating the design life of clay cut slopes. Proc Inst Civ Eng Geotech Eng 2021. https://doi.org/10.1680/JGEEN.21.00125/ASSET/IMAGES/SMALL/JGEEN.21.00125-F13.GIF.
[9] Postill H, Helm PR, Dixon N, Glendinning S, Smethurst JA, Rouainia M, et al. Forecasting the long-term deterioration of a cut slope in high-plasticity clay using a numerical model. Eng Geol 2021;280:105912.
[10] Postill H, Dixon N, Fowmes G, El-Hamalawi A, Take WA. Modelling seasonal ratcheting and progressive failure in clay slopes: A validation. Can Geotech J 2020;57:1265–79. https://doi.org/10.1139/CGJ-2018-0837/ASSET/IMAGES/CGJ-2018-0837IEQ21.GIF.
[11] Rouainia M, Helm P, Davies O, Glendinning S. Deterioration of an infrastructure cutting subjected to climate change. Acta Geotech 2020;15:2997–3016. https://doi.org/10.1007/s11440-020-00965-1.
[12] Qi G, Michel J-C, Boivin P, Charpentier S. A Laboratory Device for Continual Measurement of Water Retention and Shrink/Swell Properties during Drying/Wetting Cycles. HortSci 2011;46:1298–302. https://doi.org/10.21273/HORTSCI.46.9.1298.
[13] Romero E, Della Vecchia G, Jommi C. An insight into the water retention properties of compacted clayey soils. Géotechnique 2011;61:313–28. https://doi.org/10.1680/geot.2011.61.4.313.
[14] Wen T, Shao L, Guo X, Zhao Y. Experimental investigations of the soil water retention curve under multiple drying–wetting cycles. Acta Geotech 2020;15:3321–6. https://doi.org/10.1007/S11440-020-00964-2/TABLES/4.
[15] Romero E, Jommi C. An insight into the role of hydraulic history on the volume changes of anisotropic clayey soils. Water Resour Res 2008:44. https://doi.org/10.1029/2007WR006558.
[16] Toll D, Asquith J, Fraser A, Hassan A, Liu G, Lourenço S, et al. Tensiometer techniques for determining soil water retention curves. In: Proc. 6th Asia-Pacific Conf. unsaturated soil. CRC Press; 2015. p. 15–22. https://doi.org/10.1201/b19248-4.
[17] Mbonimpa M, Aubertin M, Maqsoud A, Bussière B. Predictive Model for the Water Retention Curve of Deformable Clayey Soils. J Geotech Geoenvironmental Eng 2006;132:1121–32. https://doi.org/10.1061/(ASCE)1090-0241(2006)132:9(1121).
[18] Wijaya M, Leong EC, Rahardjo H. Effect of shrinkage on air-entry value of soils. Soils Found 2015;55:166–80. https://doi.org/10.1016/j.sandf.2014.12.013.

[19] Tripathy S, Rao KS, Fredlund DG. Water content - void ratio swell-shrink paths of compacted expansive soils. Can Geotech J 2002;39:938–59. https://doi.org/10.1139/t02-022.
[20] Nowamooz H, Masrouri F. Relationships between soil fabric and suction cycles in compacted swelling soils. Eng Geol 2010;114:444–55. https://doi.org/10.1016/j.enggeo.2010.06.005.
[21] Estabragh AR, Parsaei B, Javadi AA. Laboratory investigation of the effect of cyclic wetting and drying on the behaviour of an expansive soil. Soils Found 2015;55:304–14. https://doi.org/10.1016/j.sandf.2015.02.007.
[22] Romero E, Gens A, Lloret A. Water permeability, water retention and microstructure of unsaturated compacted Boom clay. Eng Geol 1999;54:117–27. https://doi.org/10.1016/S0013-7952(99)00067-8.
[23] Romero E, Vaunat J. Retention curves of deformable clays. Proc an Int Work unsaturated soils, Exp Evid Theor approaches unsaturated soils 2000:91–106.
[24] Birle E, Heyer D, Vogt N. Influence of the initial water content and dry density on the soil–water retention curve and the shrinkage behavior of a compacted clay. Acta Geotech 2008;3:191–200. https://doi.org/10.1007/s11440-008-0059-y.
[25] Seiphoori A, Ferrari A, Laloui L. Water retention behaviour and microstructural evolution of MX-80 bentonite during wetting and drying cycles. Géotechnique 2014;64:721–34. https://doi.org/10.1680/geot.14.P.017.
[26] BSI. BS 1377:1990 - Methods of Test for Soils for Civil Engineering Purposes 1990.
[27] METER Group I. WP4C Dew Point PotentiaMeter Operator's Manual. 2018.
[28] Cardoso R, Romero E, Lima A, Ferrari A. A Comparative Study of Soil Suction Measurement Using Two Different High-Range Psychrometers. Exp Unsaturated Soil Mech 2007;112:79–93. https://doi.org/10.1007/3-540-69873-6_8.
[29] Romero E. A microstructural insight into compacted clayey soils and their hydraulic properties. Eng Geol 2013;165:3–19. https://doi.org/10.1016/j.enggeo.2013.05.024.
[30] Alonso EE, Cardoso R. Behavior of materials for earth and rockfill dams: Perspective from unsaturated soil mechanics. Front Archit Civ Eng China 2010;4:1–39. https://doi.org/10.1007/s11709-010-0013-6.
[31] Chen P, Lu N. Generalized Equation for Soil Shrinkage Curve. J Geotech Geoenvironmental Eng 2018;144:04018046. https://doi.org/10.1061/(ASCE)GT.1943-5606.0001889.
[32] Monroy R, Zdravkovic L, Ridely A. Evolution of microstructure in compacted London Clay during wetting and loading. Géotechnique 2010;60:105–19. https://doi.org/10.1680/geot.8.P.125.
[33] Toll DG. A conceptual model for the drying and wetting of soil. Proc First Int Conf Unsaturated Soils 1995;2:805–10.
[34] Mualem Y. Modified approach to capillary hysteresis based on a similarity hypothesis. Water Resour Res 1973;9:1324–31. https://doi.org/10.1029/WR009I005P01324.
[35] Tarantino A, De Col E. Compaction behaviour of clay. Compaction behaviour of clay Géotechnique 2008;58(3):199–213.
[36] Alonso EE, Pinyol NM, Gens A. Compacted soil behaviour: initial state, structure and constitutive modelling. Géotechnique 2013;63:463–78. https://doi.org/10.1680/geot.11.P.134.
[37] Cornelis WM, Corluy J, Medina H, Díaz J, Hartmann R, Van Meirvenne M, et al. Measuring and modelling the soil shrinkage characteristic curve. Geoderma 2006;137(1-2):179–91.
[38] Peng X, Horn R. Identifying Six Types of Soil Shrinkage Curves from a Large Set of Experimental Data. Soil Sci Soc Am J 2013;77:372–81. https://doi.org/10.2136/sssaj2011.0422.
[39] Tripathy S, Subba Rao KS. Cyclic Swell-Shrink Behaviour of a Compacted Expansive Soil. Geotech Geol Eng 2009;27:89–103. https://doi.org/10.1007/s10706-008-9214-3.
[40] Liu G, Toll DG, Kong L, Asquith JD. Matric suction and volume characteristics of compacted clay soil under drying and wetting cycles. Geotech Test J 2020;43:464–79. https://doi.org/10.1520/GTJ20170310.
[41] Bulut R, Leong EC. Indirect Measurement of Suction. Geotech Geol Eng 2008;26:633–44. https://doi.org/10.1007/s10706-008-9197-0.
[42] Marinho FAM, Take WA, Tarantino A. Measurement of Matric Suction Using Tensiometric and Axis Translation Techniques. In: Tarantino, A., Romero, E., Cui Y, editor. Lab. F. Test. Unsaturated Soils, Dordrecht: Springer, Dordrecht; n.d., p. 3–19. Doi: 10.1007/978-1-4020-8819-3_2.
[43] Smethurst J, Clarke D, Powrie W. Factors controlling the seasonal variation in soil water content and pore water pressures within a lightly vegetated clay slope. Géotechnique 2012;62:429–46. https://doi.org/10.1680/geot.10.P.097.
[44] Yu Z, Eminue OO, Stirling R, Davie C, Glendinning S. Desiccation cracking at field scale on a vegetated infrastructure embankment. Géotechnique Lett 2021;11:1–8. https://doi.org/10.1680/jgele.20.00108.
[45] Mcconnell E, Holmes J, Stirling R, Davie CT, Glendinning S. Multiscale approach to the investigation of desiccation cracking and its influence on the hydraulic regime in high plasticity clay. In: Stirling R, Nadimi S, editors. 16th BGA Young Geotech. Eng. Symp., Newcastle upon Tyne: 2022, p. 7–8.